



NUMERICAL SIMULATION OF ROTOR-FUSELAGE INTERACTION

by

B. CANTALOUBE and C. REHBACH

ONERA Office National d'Etudes et de Recherches

Aérospatiales, Châtillon, France.

**TWENTIETH EUROPEAN ROTORCRAFT FORUM
OCTOBER 4 - 7, 1994 AMSTERDAM**

ABSTRACT

An unsteady 3-D Panel Method coupled with a Lagrangian transport of the vortex sheet has been applied to compute the subsonic aerodynamics of a multi-bladed rotor.

In this paper the numerical application concerns the four-bladed rotor/fuselage configuration in forward flight studied at the University of Maryland.

Prediction of time pressure responses on two transducers located on the fuselage (under the rotor disc) agrees with Maryland wind tunnel experiments. The time evolution of the rotor thrust coefficient shows that its mean value is slightly overpredicted compared to Maryland experiments.

It is worth noting that this method does not entail any input data such as a prescribed wake or a spanwise distribution of circulation given from experiments. For this reason the method can deal with very complex rotor-fuselage interactions.

1. Introduction.

The three-dimensional behaviour of the flowfield around an helicopter is essentially due to the vortex sheets issued from rotor blades. A precise understanding of the structures of the vortex sheets, of their influence on rotor performances and of the loads they induce on the fuselage will enable to improve the performances and the handling qualities of modern helicopters. In hover and in forward flight at moderate advance ratios, the rotor-wake-fuselage interactions are of the greatest importance.

Wake influences on isolated rotors are actually well understood and modelised. Up to now rotor-wake-fuselage interaction was a problem which overtook the frame of available numerical methods. In order to make the flow computable simplifying assumptions must be made. So, recent works [1] undertaken in this area neglect compressibility and viscosity of the fluid. Thus, surface singularity methods coupled with free wake analysis can be successfully applied. Though these methods are limited with respect to the accuracy of aerodynamic phenomena computed they allow a good understanding of interaction problems. A code developed at ONERA for computing rotor performances in real flight configurations [2] has been updated and used for the rotor-wake-fuselage interaction problem.

The interaction of an isolated rotor with wakes issued from his blades has been computed using the integral method developed at ONERA. Results of an isolated rotor in hover and in climbing or descending forward flight are presented in references [3], [4] and [5].

The unsteady pressure fluctuations on the fuselage resulting from rotor-wake-fuselage interaction are evaluated in this paper. In order to minimize the CPU time, rotor blades are represented by lifting surfaces leading to a boundary problem of first order (Neumann problem [4]). The fuselage is treated with an integral boundary method of second order (Dirichlet problem [5]).

2. Theoretical background.

In this paper vorticity is discretised either by a surface repartition of doublets or by a volume repartition of vorticity. A theoretical review of these two discretisations is given below.

2.1. Surface representation of vorticity .

It is established in reference [6] that the velocity potential induced at a point P of the flow field by the rotor (surface S_R), the vortex sheets (surface S_N) and by the fuselage (surface S_F) is given by :

$$\begin{aligned}
 4\pi\Phi_P = 4\pi\Phi_\infty + \iint_{S_R} \frac{\sigma}{r} ds_Q + \iint_{S_R} \mu \vec{n}_Q \cdot \nabla_Q \left(\frac{1}{r}\right) ds_Q \\
 + \iint_{S_F} \frac{\sigma}{r} ds_Q + \iint_{S_F} \mu \vec{n}_Q \cdot \nabla_Q \left(\frac{1}{r}\right) ds_Q \\
 + \iint_{S_N} \mu \vec{n}_Q \cdot \nabla_Q \left(\frac{1}{r}\right) ds_Q
 \end{aligned} \quad (1)$$

where

$$\mu \equiv \Phi_+ - \Phi_- ,$$

$$\sigma \equiv - \vec{n} \cdot (\nabla\Phi_+ - \nabla\Phi_-)$$

and

$$r \equiv |\vec{r}| = |\vec{X}_Q - \vec{X}_P| .$$

Φ_∞ stands for the potential of the uniform flow at infinity. For thick bodies (thick blades, fuselage) \vec{n} is the unit normal vector directed towards the flow, for thin bodies (lifting surfaces, vortex sheets) \vec{n} is directed upward.

Subscript + or - allows to differentiate the value of a variable on both sides of a boundary surface S (+ side \vec{n}_+ and - side \vec{n}_-).

Subscripts P and Q designate respectively the variables associated with observation and variable points.

The variables μ and σ represent respectively a surface repartition of doublets and sources.

The velocity resulting from the potential (1) is:

$$\begin{aligned}
 4\pi\vec{V}_P \equiv 4\pi\nabla_P \Phi = 4\pi\vec{V}_\infty + \iint_{S_R} \sigma \nabla_P \left(\frac{1}{r}\right) ds_Q + \iint_{S_R} \mu \nabla_P (\vec{n}_Q \cdot \nabla_Q \left(\frac{1}{r}\right)) ds_Q \\
 + \iint_{S_F} \sigma \nabla_P \left(\frac{1}{r}\right) ds_Q + \iint_{S_F} \mu \nabla_P (\vec{n}_Q \cdot \nabla_Q \left(\frac{1}{r}\right)) ds_Q \\
 + \iint_{S_N} \mu \nabla_P (\vec{n}_Q \cdot \nabla_Q \left(\frac{1}{r}\right)) ds_Q .
 \end{aligned} \quad (2)$$

For the approximation "**thin blade**" (lifting surface) $\sigma=0$ on S_R .

The dynamic equilibrium condition for the vortex sheet (surfaces S_N)

$$\rho_+ - \rho_- = 0$$

and the unsteady Bernoulli equation yield the transport equation for doublets:

$$\frac{D\mu}{Dt} = 0 \quad (3a)$$

where

$$\frac{D}{Dt} \equiv \frac{\delta}{\delta t} + \vec{V}_m \cdot \nabla,$$

with

$$\vec{V}_m = \frac{\vec{V}_+ + \vec{V}_-}{2},$$

is standing for the convective derivative.

In order to discretise equation (2) it is worthwhile to recall the equivalence between a surface repartition of doublets (μ) and vorticity ($\vec{n} \times \nabla \mu$) [7]:

$$\iint_{S_N} \mu \nabla_P \left(\vec{n}_Q \cdot \nabla_Q \left(\frac{1}{r} \right) \right) ds_Q = - \int_{C_N} \mu \nabla_P \left(\frac{1}{r} \right) \times d\vec{l}_Q - \iint_{S_N} (\vec{n} \times \nabla \mu) \times \nabla_P \left(\frac{1}{r} \right) ds_Q$$

where C_N is the boundary of the open surface S_N . The right hand side (RHS) is the sum of two vortex velocity fields: the field due to the vortex distribution $\vec{n} \times \nabla \mu$ on S_N and the field due to a concentrated vortex filament $\mu d\vec{l}_Q$ on C_N .

The time evolution of wakes, modelised by a surface repartition of doublets, is governed by the transport equation (3a). The RHS of this equation being time independent the numerical integration is straightforward. Furthermore, this equation fulfils implicitly the Kelvin conservation theorem for the circulation. From a numerical point of view this approach raises considerable difficulties as soon as wake distortion is important. For example, a wake breaking strategy, not yet implemented in the code, would be necessary when the wake is in close proximity of the fuselage.

2.2. Volume representation of vorticity .

Using the volume representation of vorticity, the velocity potential at a point P of the flow differs from (1) only by the term relative to the vortex sheet S_N .

The relation

$$4\pi\Phi_N = \iint_{S_N} \mu \vec{n}_Q \cdot \nabla_Q \left(\frac{1}{r} \right) ds_Q , \quad (4a)$$

is replaced by :

$$4\pi\Phi_N = - \iiint_{D_\omega} \frac{(\vec{e} \times \vec{r}) \cdot \vec{\omega}}{r (r - \vec{e} \cdot \vec{r})} dv_Q \quad (4b)$$

where

$$\vec{\omega} \equiv \nabla \times \vec{V}$$

is the vortex vector contained in the domain D_ω . The relation (4b) is demonstrated in reference [8], Φ_N is called the vortex potential.

The velocity induced at a point P by the vortex sheet modelised by a surface distribution of doublets

$$4\pi\vec{V}_N = \iint_{S_N} \mu \nabla_P (\vec{n}_Q \cdot \nabla_Q \left(\frac{1}{r} \right)) ds_Q , \quad (5a)$$

becomes, for a volume repartition of vorticity :

$$4\pi\vec{V}_N = - \iiint_{D_\omega} \vec{\omega} \times \nabla_P \left(\frac{1}{r} \right) dv_Q . \quad (5b)$$

The time evolution of the vorticity $\vec{\omega}$ is governed by the Helmholtz equation :

$$\frac{D\vec{\omega}}{Dt} = (\vec{\omega} \cdot \nabla) \vec{V} , \quad (3b)$$

which is obtained by taking the curl of the Euler equations. Unlike in 2-D flow the RHS of (3b) (deformation term) is different from zero and is space and time dependent. As it was mentioned for the surface modelisation of vorticity (3a), this equation also implicitly fulfils the Kelvin conservation theorem of the circulation (the flux of $\vec{\omega}$ vector being constant through a vortex tube).

Using the scalar equation (3a) the RHS of which is zero is less expensive than using the vectorial equation (3b) with a time dependent RHS. That raises the question : **in what circumstances is it preferable to use (3b) than (3a) ?**

A jointive set of doublet panels is used for the discretisation of (3a) whereas a set of independent vortex particles is used for (3b). Hence, from a numerical point of view, the time evolution of vorticity computed from (3b) is more flexible than (3a) in the cases where the wake distortion is too important. Unlike for doublet panels, no wake breaking strategies are needed when the wake impinges the fuselage. In paragraph 3 both modelisations have been applied to the rotor-wake-fuselage interaction in forward flight.

2.3. Boundary value problem .

- Point P located on one of the blades

It is recalled that blades are represented by lifting surfaces. Thus a condition concerning the normal velocity component is imposed on surfaces S_R (Neumann boundary condition). Relation (2) gives :

$$\iint_{S_R + S_F} \mu \vec{n}_P \cdot \nabla_P (\vec{n}_Q \cdot \nabla_Q (\frac{1}{r})) ds_Q = 4\pi \vec{n}_P \cdot (\vec{V}_P - \vec{V}_\infty - \vec{V}_N) - \iint_{S_F} \sigma \vec{n}_P \cdot \nabla_P (\frac{1}{r}) ds_Q . \quad (6a)$$

- Point P located on the fuselage

A boundary condition concerning the potential on the inner face, S_{F-} , of the fuselage (Dirichlet boundary condition) is imposed. Relation (1) gives:

$$\iint_{S_R + S_F} \mu \vec{n}_Q \cdot \nabla_Q (\frac{1}{r}) ds_Q = 4\pi (\Phi_P - \Phi_\infty - \Phi_N) - \iint_{S_F} \frac{\sigma}{r} ds_Q . \quad (6b)$$

Integral relations (6a) and (6b) are written in a galilean frame in order to ensure the existence of a velocity potential. The discretisation of (6a) and (6b) gives two linear systems described in detail in [9]. In the RHS of (6a) $\vec{V}_P, \vec{V}_\infty, \vec{V}_N$ are respectively the velocity at point P, the free stream velocity and the velocity induced by the vortex domain (wake), in the RHS of (6b) $\Phi_P, \Phi_\infty, \Phi_N$ are the corresponding velocity potentials (Φ_N results from (4b) see [8]). In our problem, a convenient simplification of equations (6a) and (6b) is to take

$$\Phi_\infty = 0$$

and

$$\vec{V}_\infty = 0.$$

In (6a) and (6b) the velocity \vec{V}_N and the velocity potential Φ_N are updated, the other terms take into account the boundary conditions. Calculations are performed using a relative frame moving with the rotor. The relation between the relative velocity \vec{V}_r at point P, the absolute velocity \vec{V}_a and the driving velocity of the relative frame \vec{V}_e is given by :

$$\vec{V}_a = \vec{V}_r + \vec{V}_e$$

with

$$\vec{V}_e = \vec{V}_0 + \vec{\Omega} \times \vec{R},$$

where $\vec{\Omega}$ is the rotor instantaneous rotational velocity and $\vec{R} = \vec{OP}$, O being the center of rotation on the rotor. \vec{V}_0 is the forward flight velocity.

In the rotor attached frame the relative velocity of any point P on the blades is tangent to the blade surfaces S_R :

$$\vec{V}_r \cdot \vec{n} = 0,$$

giving

$$4\pi \vec{n}_P \cdot \vec{V}_P = 4\pi \vec{n}_P \cdot \vec{V}_e,$$

which is reported into (6a).

For the **inner potential** at a point P located on the fuselage (surface S_{F-}) there are two possibilities.

First, one may impose:

$$\Phi_P = 0.$$

In this case it has been shown in [7] that the slip condition on fuselage gives the surface distribution of sources:

$$\sigma = -\vec{n} \cdot \vec{V}_o$$

in (6a) and (6b).

The Fredholm equation of second kind (6b) gives the unknown surface density distribution of doublets μ . Then the partial derivative of the outer potential Φ_+ (on the fuselage) can be related to the solution μ :

$$\frac{\delta\Phi_+}{\delta t} = \frac{\delta\mu}{\delta t}.$$

It has been demonstrated in [6] that the equation (2) for the absolute velocity written on the fuselage reduces to:

$$\vec{V}_a = \sigma \vec{n} + \nabla\mu.$$

From definitions of partial derivative of potential, driving velocity \vec{V}_e and relative velocity \vec{V}_r , the pressure coefficient on S_F is defined as:

$$C_p = -2 \frac{\delta\Phi_+}{\delta t} + \vec{V}_e^2 - \vec{V}_r^2.$$

Second, one may impose:

$$\Phi_p = \Phi_N .$$

In this case the source density on the fuselage is :

$$\sigma = - \vec{n} \cdot (\vec{V}_o - \vec{V}_N)$$

and the partial time derivatives of potential Φ_+ on the fuselage

$$\frac{\delta\Phi_+}{\delta t} = \frac{\delta\mu}{\delta t} + \frac{\delta\Phi_N}{\delta t} .$$

Now (see [7]) the absolute velocity \vec{V}_a may be related to the density of doublet μ , of source σ and to the vortex velocity \vec{V}_N as follows:

$$\vec{V}_a = \sigma \vec{n} + \nabla\mu + \vec{V}_N .$$

3. Rotor-wake-fuselage interaction in forward flight.

The numerical results presented herein show that the integral method is of a great versatility for computing very complex flows such as the rotor-wake-fuselage interaction. The configuration studied here is that of reference[1]. The general arrangement of the rotor and fuselage is shown on figure 1. The geometric characteristics of the rotor and flight parameters are reported bellow.

3.1. Rotor geometry and flight parameters.

number of blades : 4
 Blade chord c: 0.0635 m
 Rotor radius R : 0.8255 m
 blade root R_0 : 0.2060 m
 blade profile : unsymmetric OA209
 blade taper ratio : 1
 rotor solidity σ : 0.097941
 blade linear twist : -12°
 Mach number at the tip of the blade : 0.472
 shaft tilt angle α_Q : -6°
 advance ratio μ : 0.100
 collective pitch angle θ_0 : 9.039°
 cyclic pitch angle θ_c : -5.412°
 θ_s : 0.152°
 cyclic flapping angle β_0 : 3.00°
 β_c : 0°
 β_s : 0°

The cyclic pitching and flapping laws via azimuth are :

$$\theta = \theta_0 + \theta_c \cos (\psi) + \theta_s \sin (\psi) ,$$

$$\beta = \beta_0 + \beta_c \cos (\psi) + \beta_s \sin (\psi) .$$

3.2. Numerical results.

In reference [1] it has been shown that the signature of the pressure on the fuselage is strongly affected by the passage of the blades and by the vortex sheets issued from the rotor. The passage of the blades produces a pulse which varies in phase whereas the vortex sheet interaction is characterised by a non phased response with respect to the blade azimuth.

In the present paper we do not take into account the direct wake impingement and downstream wake impingement effects (mentioned in [1]) on the pressure.

From O. Rand [10] only the blade passage phenomenon can be realistically modelised by means of an incompressible and inviscid fluid theory such as the unsteady 3-D Panel Method presented here.

The time pressure evolution C_p^u will be computed about its mean value on the fuselage at locations 1 and 5 (see fig. 2). The point 1 is located on the body nose where the vortex sheet deformation (tearing) effect will be of less importance than the blade passage effects. On the contrary, the pressure response at the point 5, located on the rear part of the fuselage, will be affected either by the vortex sheets and the blade passage.

The modelisation of the wake has been made by using either a surface repartition of doublets (**results a**) or a volume repartition of vorticity (**results b**). For the first case (**results a**) the boundary condition on the inner part of the fuselage is $\Phi_{-F} = \Phi_F$ and for the second case (**results b**) this condition is $\Phi_{-F} = 0$.

On figures 3 and 4 the pressure signature at points 1 and 5 obtained from Maryland experiment [1] is compared with **results a**. Figure 3 shows that the pressure response at point 1 is smooth and agrees quite well with Maryland experiment, the peak pressures are slightly underpredicted but the phase is correctly evaluated. It is worth noting that the helicopter (fuselage and rotor) is impulsively started from rest and that the flow reaches its established periodic state nearly one rotor turn later. On figure 4, the pressure agrees very well with the experiment. During the first turn of the rotor the flow is setting up. From azimuth 300 to 600 degrees the periodic state compares well with experiments. The oscillations appearing after this azimuth are due to numerical difficulties as the vortex sheet modelising the wake comes too close to the fuselage. As is pointed out in [11], this drawback, inherent to the surface doublet representation of the wake, can be overcome by stretching and even by artificially breaking the wake in the vicinity of the fuselage. Nevertheless in the present results (**results a**) no particular treatment has been applied.

Figures 5 and 6 compare unsteady pressure coefficients measured at points 1 and 5 with the numerical results obtained by a volume repartition of vorticity (**results b**) for the second turn of the rotor. Agreement in amplitude and in phase are satisfactory. We notice that the curves are less smooth than for **results a**. The irregularities observed are due to the vortex-point discretisation of the wake (particles). The cut-off function applied on the induction law for each particle cannot smooth entirely the pressure response at points too close to a particle.

These results show the great versatility of the vortex-point discretisation of the wake when it is strongly stretched or broken by an obstacle (fuselage). Indeed the induction law (Biot and Savart) does not take into account the relative position of the particles from each other. Thus, no breaking strategy is needed when the wake passes close to the fuselage. Even after the second turn of the rotor the pressure response can be computed and is in good agreement with the experiment.

The figure 7 shows the time evolution of the thrust coefficient. After one turn of the rotor the periodic state is reached. Its overprediction is due to a lower blade linear twist (-12° instead of -13° in the experiment) and to some geometric modification in the vicinity of the blade root.

The wake (surface-doublet modelisation) issued from the blade located over the rear part of the fuselage is represented on figure 8. This picture gives a hint of the breaking strategy which should be adopted in future work.

The CPU cost is 4620 seconds for the first turn of the rotor on a CRAY-YMP ($6 \times 60 = 360$ vortex particles have been created). For the second turn the CPU time is 9720 seconds.

4. Conclusion .

The present results show that the boundary integral method used here is well suited to predict correctly the blade passage effects. The numerical treatment of the interaction of vortex-sheets with the fuselage which is far from being straightforward is underway by solving a type 2 Fredholm integral equation for the total pressure [12].

References .

- [1] G.L. Crouse , J.G. Leishman , N. Bi
Theoretical and experimental study of unsteady rotor/body aerodynamic interactions.
46th Annual Forum of the American Helicopter Society , Washinton D.C. ,
May 1990 .
- [2] B. Cantaloube
Numerical calculation of rotor performances in real flight configurations.
International Conference on Rotor Basic Research , Research Triangle Park ,
North Carolina , February 1985 .

- [3] C. Rehbach
Calcul d'un rotor d'hélicoptère en vol stationnaire par une méthode intégrale .
Note Technique ONERA no. 23/1737 AN -Novembre 1991 .
- [4] C. Rehbach
Calcul d'un rotor d'hélicoptère en vol d'avancement par une méthode intégrale .
Note Technique ONERA no. 24/1737 AN -Juillet 1992 .
- [5] C. Rehbach
Calcul d'un rotor d'hélicoptère en vol de descente par des méthodes intégrales .
Rapport de Synthèse Final ONERA no. 25/1737 AY -Avril 1993 .
- [6] B. Hunt
The mathematical basis and numerical principles of the boundary integral
method for incompressible potential flow over 3-D aerodynamic configurations
Numerical Methods in Applied Fluid Dynamics. Edited by B. Hunt.
Academic Press. London. 1980.
- [7] J.L. Hess
Calculation of potential flow about arbitrary three-dimensional lifting bodies .
Report No. MDC - J0545 , December 1969 .
- [8] J.-P. Guiraud
Potentiel des vitesses créées par une distribution localisée de tourbillons .
La Recherche Aérospatiale , no.1978-6 , Novembre - Décembre .
- [9] B. Cantaloube , S. Huberson
Calcul d'écoulements de fluide incompressible non visqueux autour de
voilures tournantes par une méthode particulière .
La Recherche Aérospatiale , no.1984-6 , Novembre - Décembre .
- [10] O. Rand
The influence of interactional aerodynamics in rotor/fuselage coupled response .
Proceedings of the 2th International Conference on Rotorcraft Basic Research ,
College Park , MD , 1988 .
- [11] D.R. Clark , B. Maskew
A re-examination of the aerodynamics of hovering rotors-including the presence
of the fuselage .
International Technical Specialist's Meeting on Rotorcraft Basic Research ,
Atlanta , GA , March 1991 .
- [12] B. Cantaloube , C. Rehbach
Computation of the pressure in an incompressible rotational flow of inviscid
fluid.
La Recherche Aérospatiale , no.1988-2.

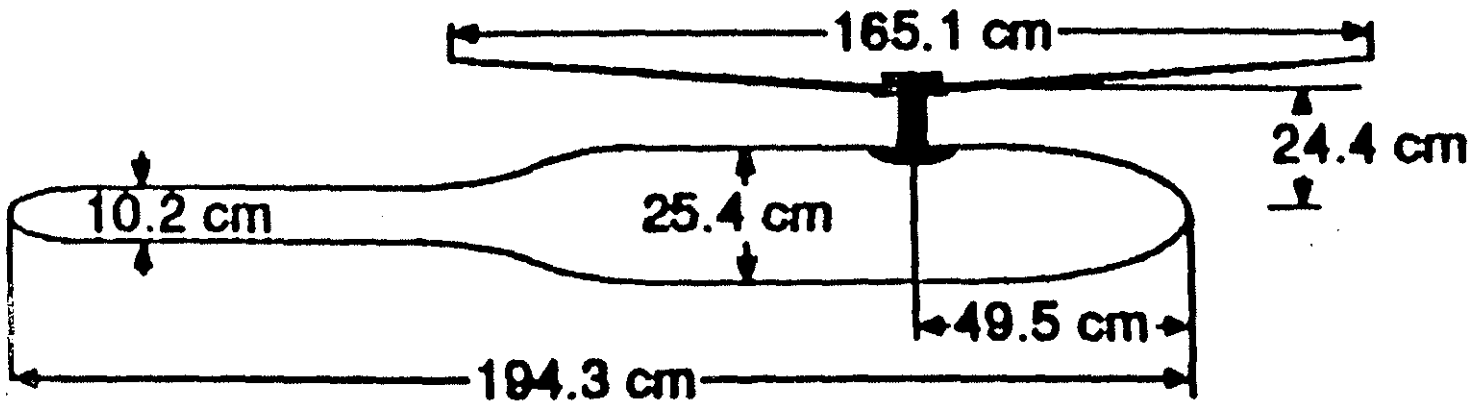


Fig.1 Rotor-fuselage arrangement

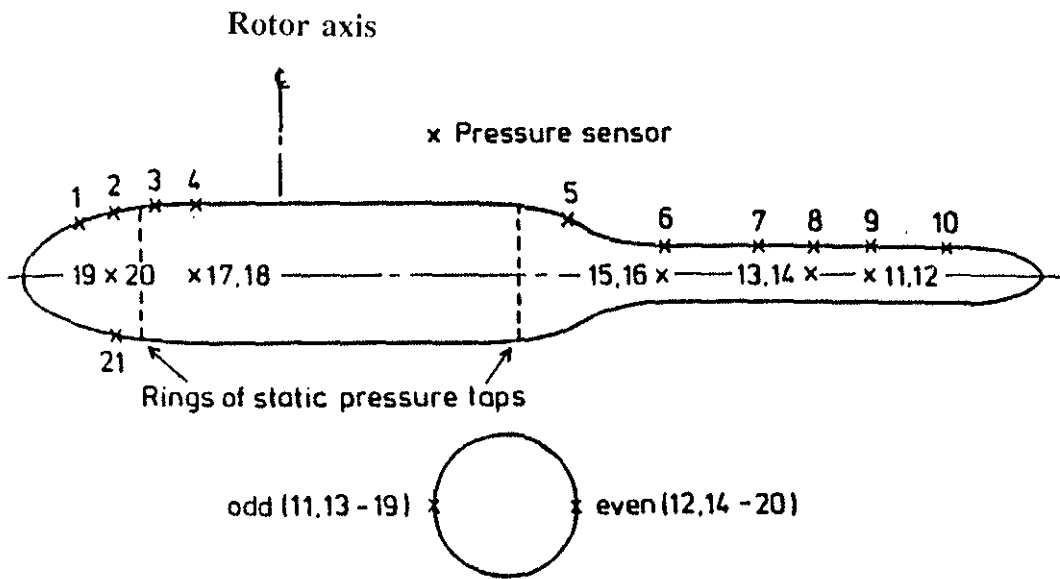


Fig. 2 Position of pressure sensors

—+1
*.....*2

Maryland experiment $\mu=0.1$, $CT/\sigma=0.091$
ONERA Results

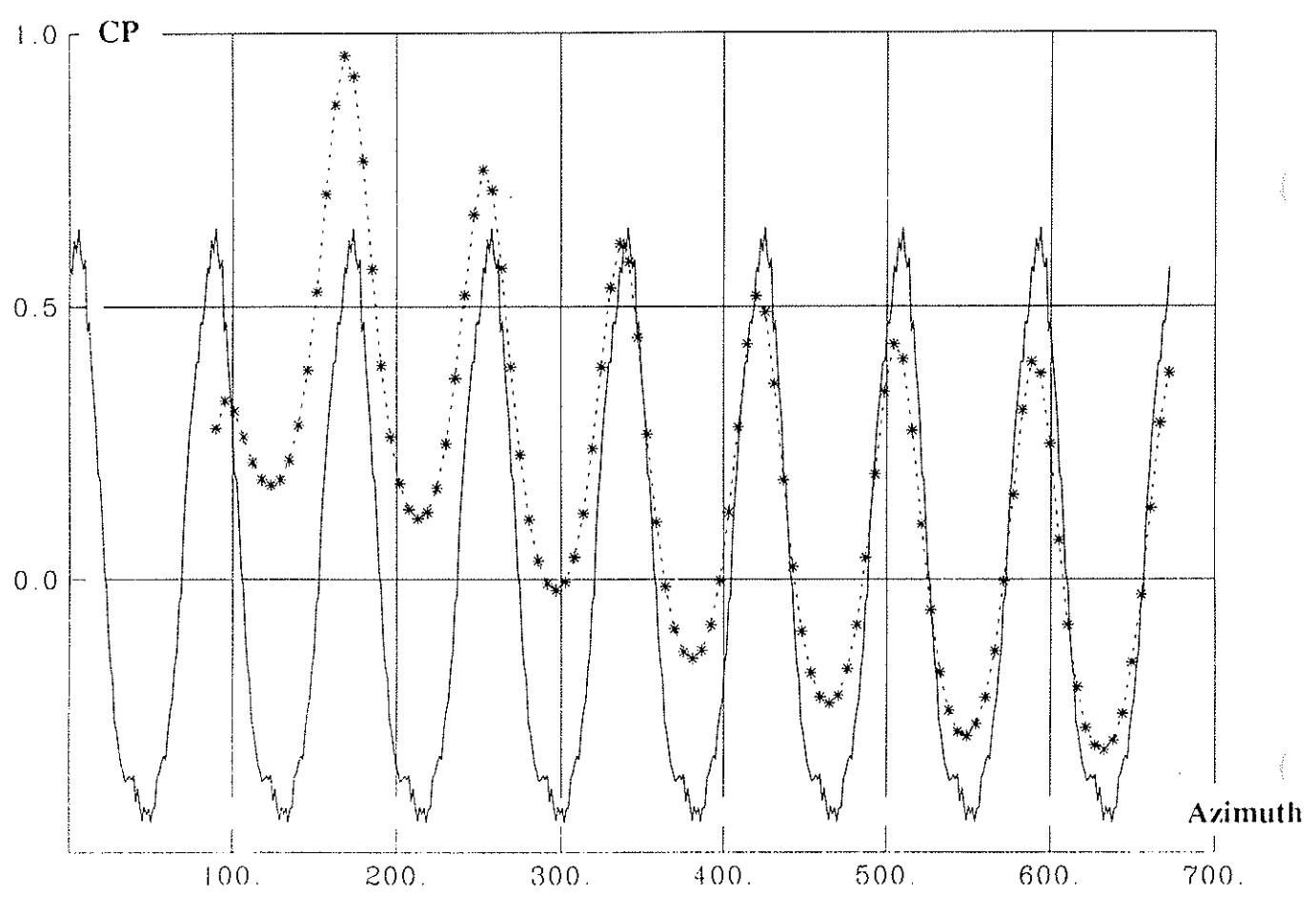


Fig.3 Unsteady pressure response (sensor 1)

—+— 1
..... 2

Maryland experiment $\mu=0.1$, $CT/\sigma=0.091$
ONERA Results

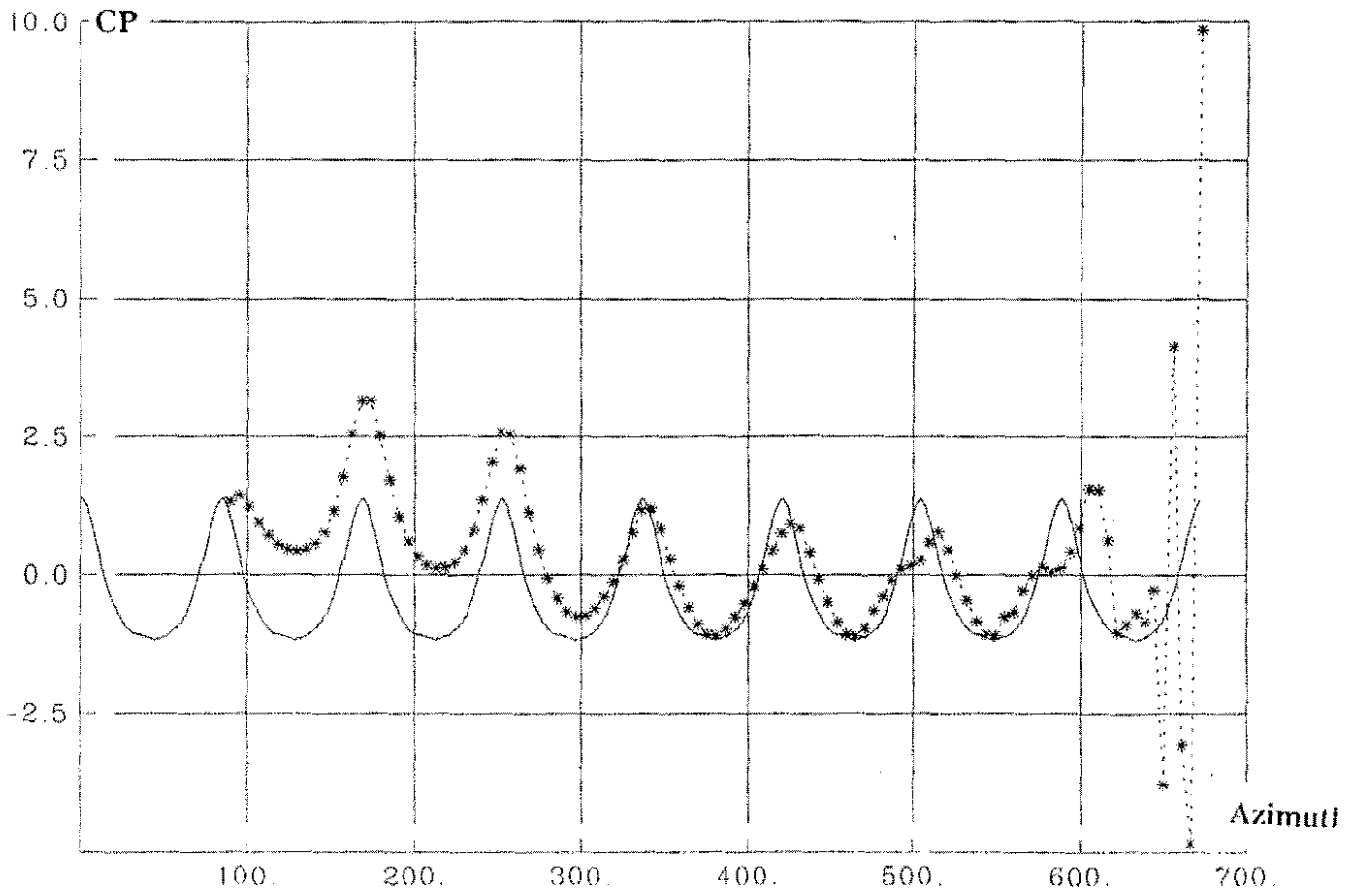


Fig. 4 Unsteady pressure response (sensor 5)

+——+ 1
..... 2

Maryland experiment $\mu=0.1$, $CT/\sigma=0.091$
ONERA Results (TPI)

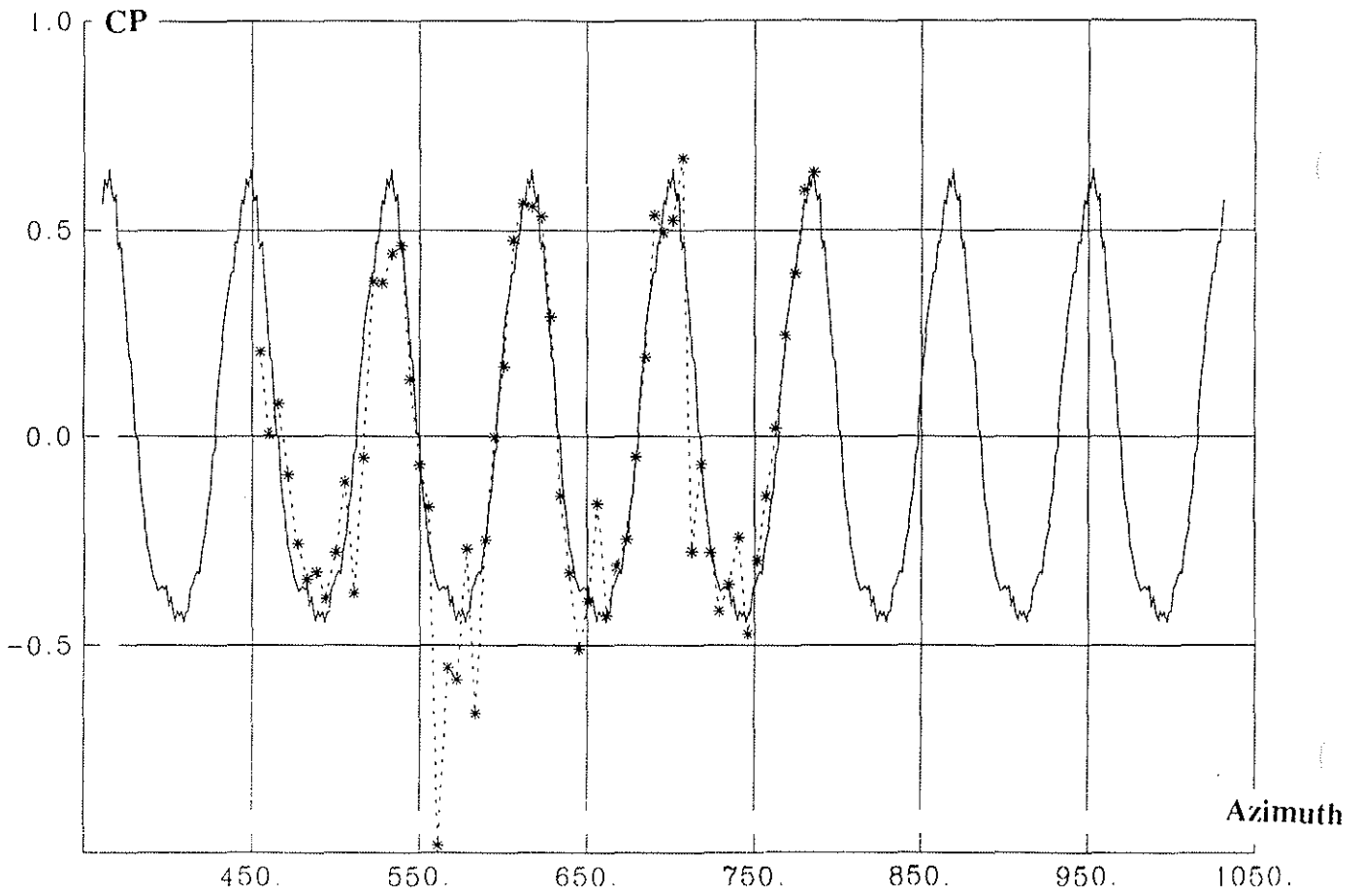


Fig. 5 Unsteady pressure response (sensor 1)

— 1
* - - - * 2

Maryland experiment $\mu=0.1$, $CT/\sigma=0.091$
ONERA Results (TPI)

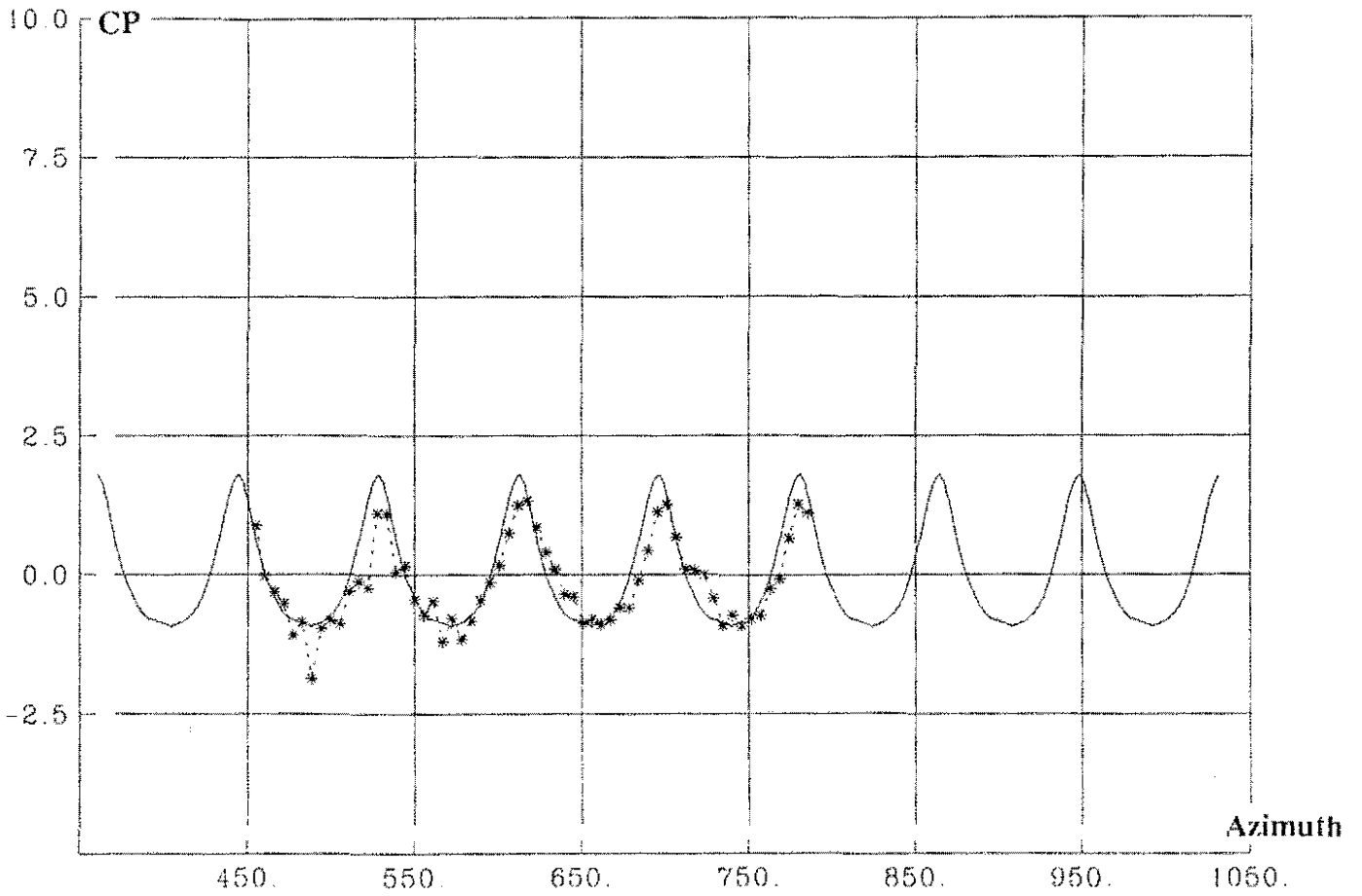


Fig. 6 Unsteady pressure response (sensor 5)

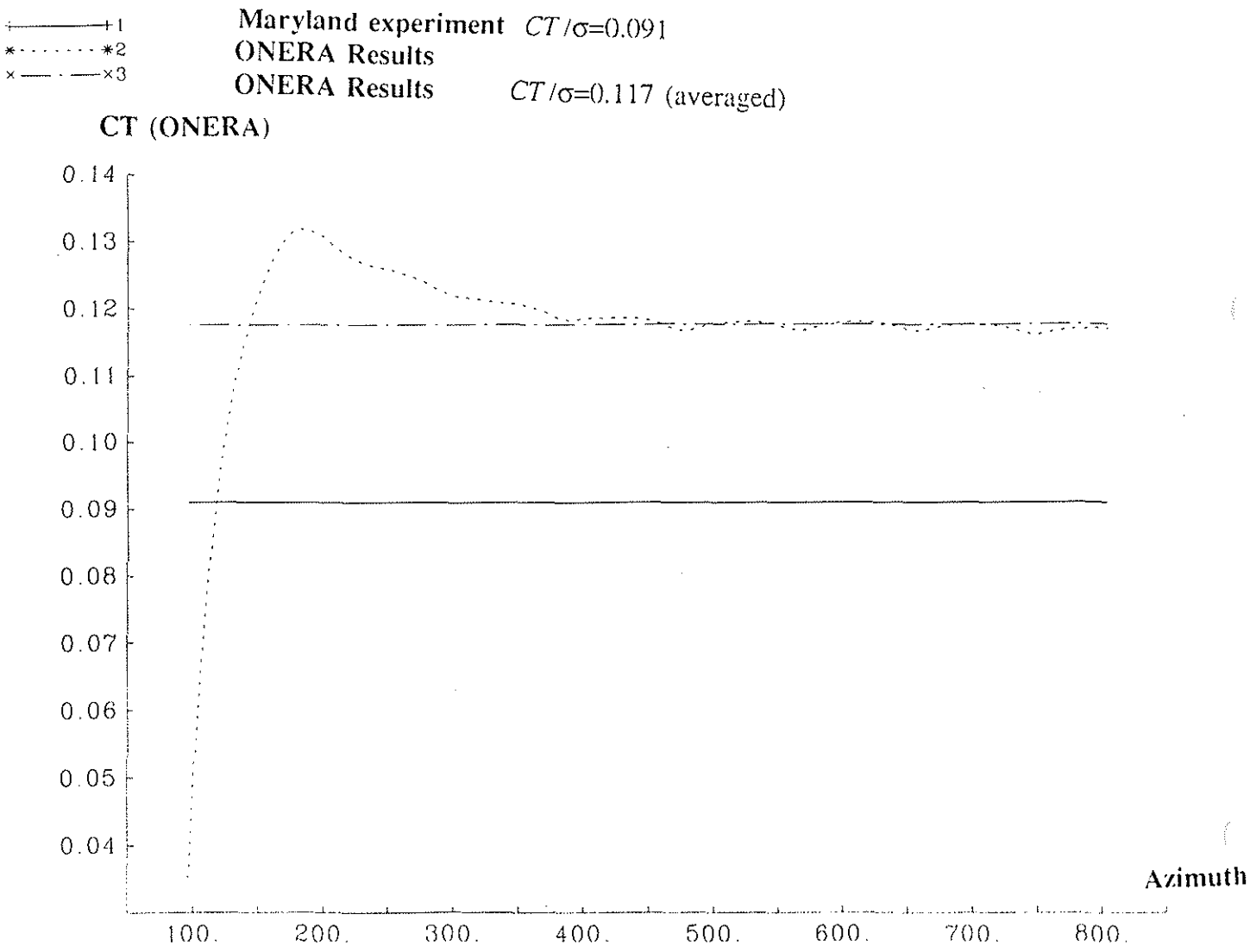


Fig. 7 Rotor thrust coefficient vs azimuth

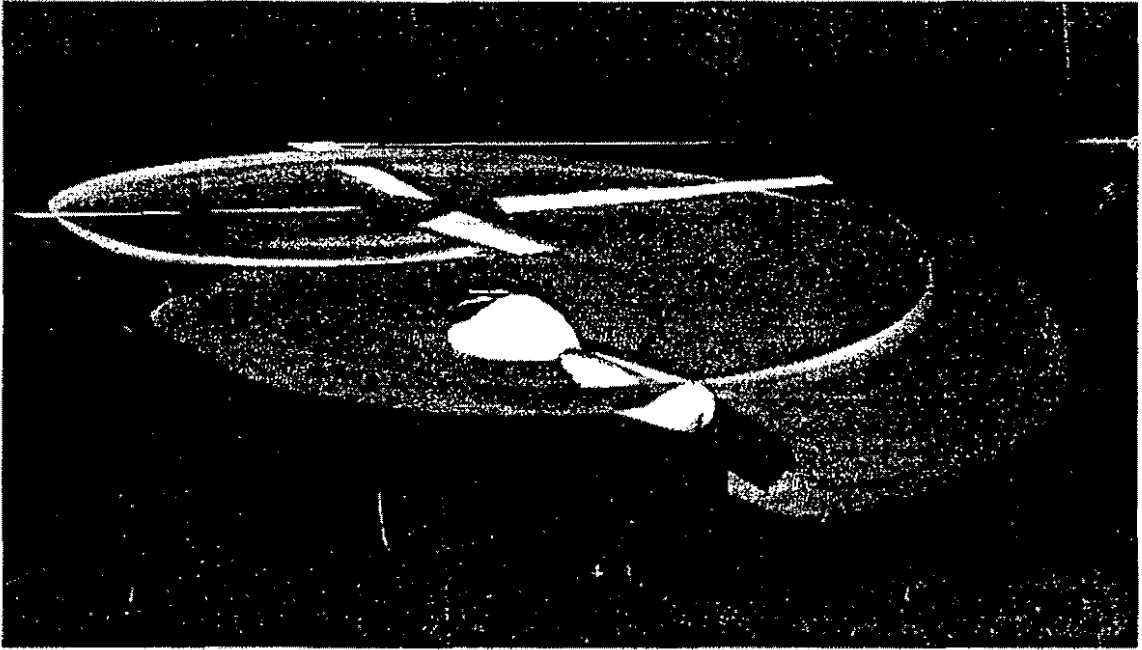


Fig.8 Calculated wake issued from the rear blade